

UV and visible activation of Cr(III)-doped TiO₂ catalyst prepared by a microwave-assisted sol–gel method during MCPA degradation

S. Y. Mendiola-Alvarez¹ · J. L. Guzmán-Mar¹ · G. Turnes-Palomino² · F. Maya-Alejandro² · A. Hernández-Ramírez¹ · L. Hinojosa-Reyes¹

Received: 29 June 2016 / Accepted: 1 November 2016 / Published online: 10 November 2016
© Springer-Verlag Berlin Heidelberg 2017

Abstract Photocatalytic degradation of 4-chloro-2-methylphenoxyacetic acid (MCPA) in aqueous solution using Cr(III)-doped TiO₂ under UV and visible light was investigated. The semiconductor material was synthesized by a microwave-assisted sol–gel method with Cr(III) doping contents of 0.02, 0.04, and 0.06 wt%. The catalyst was characterized using X-ray powder diffraction (XRD), scanning electron microscopy (SEM), nitrogen physisorption, UV–Vis diffuse reflectance spectroscopy (DRS), and atomic absorption spectroscopy (AAS). The photocatalytic activity for the photodegradation of MCPA was followed by reversed-phase high-performance liquid chromatography (HPLC) and total organic carbon (TOC) analysis. The intermediates formed during degradation were identified using gas chromatography–mass spectrometry (GC–MS). Chloride ion evolution was measured by ion chromatography. Characterization results showed that Cr(III)-doped TiO₂ materials possessed a small crystalline size, high surface area, and mesoporous structure. UV–Vis DRS showed enhanced absorption in the visible region as a function of the Cr(III) concentration. The Cr(III)-doped TiO₂ catalyst with 0.04 wt% of Cr(III) was more

active than bare TiO₂ for the degradation of MCPA under both UV and visible light. The intermediates identified during MCPA degradation were 4-chloro-2-methylphenol (CMP), 2-(4-hydroxy-2-methylphenoxy) acetic acid (HMPA), and 2-hydroxybuta-1,3-diene-1,4-diyl-bis (oxy)dimethanol (HBDM); the formation of these intermediates depended on the radiation source.

Keyword Heterogeneous photocatalysis · MCPA · Microwave-assisted sol–gel method · Cr(III)-doped TiO₂

Introduction

Chlorophenoxy acid herbicides such as 4-chloro-2-methylphenoxyacetic acid (MCPA) are widely used for the control of annual and perennial weeds in cereals and grass seed crops. This pesticide has been detected in groundwater, effluents of wastewater treatment plants, and agricultural drainage water (Gimeno et al. 2014; Kaminski et al. 2014). MCPA is one of the most frequently identified organic substances in groundwater and drinking water due to its poor biodegradability, high solubility, and mobility (Zertal et al. 2004). A World Health Organization (WHO) and U.S. Environmental Protection Agency (EPA) regulation set the maximum contaminant level of this compound in drinking water in 2 µg/L (United States Environmental Protection Agency 2004; WHO 2006).

Thus, alternative treatment technologies to remove MCPA from contaminated water are needed. The degradation of this compound has been described using chemical, photochemical, and biological processes (García-Segura et al. 2011; Gimeno et al. 2014; Kamaraj et al. 2014; Kaminski et al. 2014; Muter et al. 2014; Sanchis et al. 2013), but some of these treatment procedures require long treatment periods

Communicated by: Philippe Garrigues

Electronic supplementary material The online version of this article (doi:10.1007/s11356-016-8034-x) contains supplementary material, which is available to authorized users.

✉ L. Hinojosa-Reyes
laura.hinojosary@uanl.edu.mx

¹ Facultad de Ciencias Químicas, Universidad Autónoma de Nuevo León, UANL, Cd. Universitaria, C.P. 66455 San Nicolás de los Garza, Nuevo León, Mexico

² Department of Chemistry, University of the Balearic Islands, 07122 Palma de Mallorca, Spain

and in practice, are often difficult to apply in waste disposal. TiO₂-mediated heterogeneous photocatalysis has been shown to be an efficient way for complete degradation and mineralization of organic pollutants such as MCPA under UV radiation (Djebbar et al. 2006; Zertal et al. 2004). However, the activation of TiO₂ is limited only to ultraviolet light (which accounts for just 5% of the solar spectrum) due to its large band gap energy (3.2 eV). Therefore, the effective utilization of visible light for photocatalytic processes has become the ultimate goal (Daghrir et al. 2013; Devi and Kavitha 2013; Pelaez et al. 2012). Doping a TiO₂ matrix with transition metal ions has been frequently considered to be a way to improve the photocatalytic efficiency of TiO₂. Transition metal ions act as trapping sites by accepting the photogenerated electrons or holes from the TiO₂, suppressing charge carrier recombination and facilitating the onset shift in the band gap absorption to the visible region, thus improving the photocatalytic activity of the material (Devi and Kumar 2011; Dong et al. 2015; Pelaez et al. 2012). Among these dopants, Cr(III) is an interesting option, as it has an ionic radius (0.76 nm) very similar to that of Ti(IV) (0.75 nm), which could penetrate into the TiO₂ crystal lattice and easily occupy the position of Ti(IV) in the TiO₂ lattice (Peng et al. 2012; Tian et al. 2012). Furthermore, the TiO₂ doped with 3d-transition metal ions such as Cr(III) could present energy levels inside the band gap leading to significant visible light absorption for TiO₂ (Michalow et al. 2013; Ould-Chikh et al. 2014). However, photocatalytic activity usually depends on the nature and the amount of doping agent and the synthesis procedure (Devi and Kumar 2011; Michalow et al. 2013; Pelaez et al. 2012). In previously reported studies, Cr(III)-doped TiO₂ has been synthesized via different methods such as hydrothermal process (Li et al. 2013; Ould-Chikh et al. 2014), sol-gel method (Fan et al. 2008; Jaimy et al. 2011; Peng et al. 2012), and flame spray pyrolysis (FSP) (Michalow et al. 2013; Tian et al. 2012).

Among the different synthetic procedures, the sol-gel process has recently gained increasing importance in the materials science field and represents one of the simplest and cheapest methods used for TiO₂ metal ion doping (Daghrir et al. 2013; Gupta and Tripathi 2012). The main advantages of this process are high purity and homogeneity of the products obtained and that the incorporation of dopant ions is performed on the molecular scale. In addition, this method readily controls the size, shape, and size distribution of prepared catalysts (Gupta and Tripathi 2012). Recently, a microwave-assisted synthesis has been successfully applied for the preparation of different nanomaterials. Some of the advantages of the microwave-assisted methods, compared with other preparation procedures, are rapid heating, higher reaction rates, shorter reaction time, homogeneous heat transfer, phase purity, and improved yields (Pan et al. 2013; Wu et al. 2013; Wu and Tai 2013).

Thus, this research aims to study the degradation of MCPA in aqueous solution under UV and visible light using a Cr(III)-doped TiO₂ photocatalyst. The evaluated catalysts were synthesized by a microwave-assisted sol-gel method. Characterizations were performed using X-ray diffraction (XRD), nitrogen physisorption, scanning electron microscopy (SEM), UV-Vis diffuse reflectance spectroscopy (DRS), and atomic absorption spectroscopy (AAS). The influence of dopant loading and catalyst amount was investigated. Finally, gas chromatography-mass spectrometry (GC-MS) was used for the determination of organic intermediates, and ion chromatography was used to monitor the chloride ions generated as end-product during the degradation reaction of this pollutant.

Experimental procedure

Reagents

All chemicals were of analytical grade quality. Ultrapure water from a Milli-Q system (18 MΩ cm, Millipore, Bedford, MA, USA) was used to prepare the solutions. MCPA (99.8%) and 4-chloro-2-methylphenol (CMP, 97%) were purchased from Sigma-Aldrich (St. Louis, MO, USA). Standard stock solutions (100 mg/L) of MCPA and CMP were prepared using ultrapure water and stored at 4°C in dark glass bottles. Titanium (IV) isopropoxide (97%) and chromium (III) nitrate nonahydrate (99%) obtained from Sigma-Aldrich were used as precursors for the synthesis of TiO₂ nanomaterials. Titanium dioxide P25 with a composition of 80% anatase and 20% rutile was purchased from Degussa Chemicals (Hanau, Germany).

Catalyst synthesis

A microwave-assisted sol-gel method was adopted for the synthesis of both the undoped TiO₂ and the Cr(III)-doped TiO₂ materials (0.02, 0.04, and 0.06 wt%). For the synthesis, 5 mL of ultrapure water adjusted to pH 3 and 12 mL of isopropanol was mixed into a 100-mL Pyrex beaker and placed under magnetic stirring for 90 min. The corresponding quantity of Cr(NO₃)₃•9H₂O was dissolved in 5 mL of water and 4 mL of isopropanol, and the obtained solution was then slowly added drop wise at the same time as 21 mL of titanium (IV) isopropoxide to the water:isopropanol mixture. The stirring was stopped after 2 h, and the resulting mixture was irradiated in an 1800-W microwave oven with temperature controller (MARS 6, CEM) for 60 min at 150°C using 75-mL-capacity Teflon vessels. To obtain the catalyst powder, the mixture was filtered, washed with distilled water, and dried at 80°C for 20 h. The dried product was then calcined (Barnstead Thermolyne) at 500°C for 4 h (2°C/min ramp rate). The prepared materials were named 0.02-CrTi, 0.04-CrTi, and

0.06-CrTi, where the numbers correspond to the wt% composition of Cr(III) in the prepared materials. The bare TiO₂ was obtained by the same procedure with no addition of Cr(NO₃)₃•9H₂O and was named Ti.

Characterization

The particle morphology was analyzed by SEM using a JEOL JSM6510-LV microscope operated at 5 keV. The structural characterization of the catalysts was examined by XRD performed on a Siemens D5000 instrument. The diffractograms were recorded over an angular range of 10–90° (2θ) using Cu Kα radiation. The Debye–Scherrer equation (Eq. 1) was applied to the most intense peak to calculate the average crystallite size:

$$D = \frac{k\lambda}{\beta \cos\theta} \quad (1)$$

where D is the average crystallite size, k is the Scherrer constant, which is usually taken as 0.94, λ is the wavelength of the X-ray radiation, β is the half-height width of the (101) anatase diffraction peak, and θ is the diffraction angle.

The nitrogen physisorption measurement was carried out to determine the specific surface area using the Brunauer–Emmett–Teller (BET method) in a Quantachrome Autosorb-1 analyzer. The samples were degassed at 473 K prior to the measurements. The band gap energy of the photocatalysts was determined by UV–visible light DRS using a scanning UV–Vis spectrophotometer (Thermo Fisher Scientific—Evolution 300 PC) equipped with an integrating sphere TFS-Praying Mantis accessory (BaSO₄ Spectralon was used as reference). The band gaps were calculated for the samples by using the Kubelka–Munk function based on the following equation as previously described (López and Gómez 2011):

$$F(R) = \frac{(1-R)^2}{2R} \quad (2)$$

where R is reflectance of the sample and $F(R)$ is proportional to the extinction coefficient (α).

The chemical composition of the materials was determined by atomic absorption spectroscopy (AAS) (Varian SpectrAA 220 FS) using a PHOTRON hollow cathode chromium lamp after microwave-assisted acid digestion of the sample with HF:HNO₃:HCl (1:3:1) at 180°C for 20 min.

Photocatalytic evaluation

The experimental setup for photocatalytic degradation of MCPA by Cr(III)-doped TiO₂ under visible or UV radiation is schematically shown in electronic supplementary material (Fig. Sup. 1). The degradation was performed in a batch reactor (Pyrex beaker) containing 450 mL of 10 mg/L MCPA

aqueous solution and 1 g/L of catalyst loading. The photocatalytic activity was evaluated at pH 3.5, and the aqueous solution was previously adjusted at the desired pH with 1 M HNO₃ using a pH/ISE meter Orion Star A111 (Thermo Scientific). The MCPA solution was magnetically stirred, and before irradiation, the suspension was stirred in the dark for 1 h to ensure the adsorption–desorption equilibrium. Then, it was irradiated with visible radiation (Spectroline 450 nm, 358 W/m²) or UV radiation (Philips Hg lamp 365 nm, 800 W/m²). The lamp was positioned 10.0 cm above the photo-reactor, and the experiments were performed at room temperature (23 ± 2°C). The reaction rate was followed by taking aliquots at desired time intervals and then filtered. Monitoring of MCPA degradation was followed by reversed-phase high-performance liquid chromatography (HPLC, YL 900) using a Luna C8 100 × 4.6 mm, 3-μm column (Phenomenex) and a mobile phase of 50:50 (v/v) acetonitrile:water at pH 3 adjusted with H₃PO₄. The chromatographic conditions were adapted from a previous study (Solís et al. 2015). The total organic carbon concentration (TOC) during the degradation process was determined in the aqueous solution using a TOC-V CSH Shimadzu Analyzer. The intermediates 4-chloro-2-methylphenol (CMP), 2-(4-hydroxy-2-methylphenoxy) acetic acid (HMPA), and 2-hydroxybuta-1,3-diene-1,4-diyl-bis(oxy) dimethanol (HBDM) were analyzed by using a Hewlett–Packard (Agilent Technologies, Palo Alto, CA, USA) HP 7890 series GC equipped with a split/splitless injector and a mass selective detector (HP 5973C). Analytes were separated using 30 m × 0.25 mm, 0.25-μm-thick HP5MS (methyl 5% phenyl polysiloxane) gas chromatographic column (Agilent Technologies) with the following oven temperature program: initially 70°C (holding 1 min), increased at 25°C/min to 180°C, then increased to 250°C at a rate of 5°C/min, and held 1 min, with a total run of 20.4 min. Helium (99.999%) was used as the carrier gas at the flow rate of 1 mL/min. The injection port was operated in pulsed splitless mode with an injection temperature of 250°C using 1 μL sample volume injection to obtain the mass spectra (40–650 m/z). The MS was operated at the electron impact (EI) mode (70 eV). The quadrupole mass analyzer, EI ion source, and the interface temperatures were maintained at 150, 230, and 280°C, respectively.

Prior to the determination, solid-phase extraction of 1.5 mL of the sample, previously filtered, was carried out with OASIS HLB filters preconditioned with ethyl acetate, methanol, and Milli-Q water (3 mL of each) at pH 3. The sample was eluted with 3 mL of ethyl acetate, dried with N₂ gas, and reconstituted with 1 mL of ethyl acetate. The extract was treated with 200 μL of *N*-methyl-*N*-(*tert*-butyldimethylsilyl)trifluoroacetamide (MTBSTFA) as silylating reagent (Rodríguez Pereiro et al. 2004). Chloride ion determination was carried out by ionic chromatography (Dionex ICS-1100, Thermo Scientific) with a Dionex Ion

Pac® AS23 column (250 × 4 mm); the mobile phase used was 4.5 mM Na₂CO₃:0.8 mM NaHCO₃ at a flow rate of 1.2 mL/min.

Results and discussion

Characterization of catalysts

The results of the chromium content, the BET specific surface area, the crystallite size, and the E_g values of the different catalyst samples are presented in Table 1. The XRD patterns of the undoped and Cr(III)-doped samples (Fig. 1) showed that all the samples consisted of anatase as a unique crystalline phase (JCPDS, No. 21-1272). No crystalline phases involving chromium oxides or oxyhydroxide were detected, implying that Cr(III) could be incorporated into the crystal lattice of TiO₂ thanks to the similarity of the Cr(III) and Ti(IV) ionic radii (Peng et al. 2012; Tian et al. 2012). It is feasible that Cr(III) could replace Ti(IV) in the TiO₂ lattice structure (Li et al. 2013).

The results are shown in Table 1. As the dopant concentration increased, the crystallite size decreased and ranged from 20 to 14 nm. This result suggested that dopant could restrain the growth of TiO₂ crystallites introducing defects within the TiO₂ crystal lattice (Li et al. 2013).

Usually, high specific surface areas are related to small crystallite size and could have a positive effect on enhancing the reactivity of TiO₂ for photocatalytic applications. The presence of Cr (III) on the TiO₂ slightly increased the BET specific surface area from 51 to 60 m²/g, as shown in Table 1. However, surface area values were only slightly affected by the Cr(III) content. All the samples presented pore diameters (5.6–6.5 nm) within the mesoporous range (type IV isotherms).

UV–Vis diffuse reflectance spectra were recorded to determine the effect of metal doping on the TiO₂ absorption edge (Fig. 2). As seen in Table 1, increasing the amount of Cr(III) incorporated did not affect the intrinsic band gap of anatase TiO₂. However, a slight increase in the absorbance capacity at approximately 450 nm was observed in the case of the sample doped with the highest Cr(III) amount (0.06-CrTi material). This behavior can be attributed to the interfacial charge transfer from Cr(III) to the conduction band of Ti(IV) and partially to the $^4A_2g \rightarrow ^4T_1g$ transition band of Cr(III) in an octahedral coordination (Jaimy et al. 2011; Ould-Chikh et al. 2014; Tian et al. 2012). The enhancement of absorbance in the visible region could improve the photocatalytic activity of TiO₂ under visible light, as previously reported by other authors (Jaimy et al. 2011; Li et al. 2013; Ould-Chikh et al. 2014; Tian et al. 2012).

The SEM micrographs of the catalysts (Fig. 3) showed that the samples were formed by agglomerates of sphere-like-

shaped nanoparticles with diameters ranging from 50 to 90 nm. The SEM images indicated that the increment of Cr(III) content from 0 to 0.06 wt% caused the reduction of the particle size while nanoparticles become more spherical. Additionally, the increment of Cr doping in TiO₂ reduced agglomeration of particles obtaining highly dispersed TiO₂ crystals that could present high photocatalytic activity. The effect of chromium doping in the morphological properties of TiO₂ anatase structure has been previously described by Vijayalakshmi and Jereil (Vijayalakshmi and Jereil 2015). The AAS results confirmed the presence of chromium in all the prepared photocatalysts, although, as seen in Table 1, the quantity of chromium incorporated was always lower than the expected theoretical percentage value.

Photocatalytic activity of Cr(III)-doped TiO₂ catalysts

Photocatalytic activity of the undoped and the Cr(III)-doped TiO₂ catalysts was evaluated by the degradation, under visible irradiation, of MCPA solutions at pH 3.5 (natural pH of MCPA solution) using 1 g/L of catalyst loading (Fig. 4). It can be clearly seen that 0.04-CrTi showed better performance on the degradation of MCPA in comparison with either the bare TiO₂ (Ti) or Cr-doped TiO₂ materials with Cr contents of 0.02 and 0.06 wt% (Fig. 5). Thus, the optimal Cr doping level into TiO₂ to obtain the highest photocatalytic activity was 0.04 wt%, resulting in complete MCPA degradation in 240 min under visible radiation. Appropriate Cr(III)-doping levels in TiO₂ could effectively enhance the separation of the electron-hole pairs by the entry of chromium ions into the crystal lattice of TiO₂, improving its photocatalytic performance. However, an excess chromium content could be in the form of an oxide on the surface of TiO₂, where Cr(III) ions could act as recombination centers, which decrease the photoactivity of TiO₂ (Fan et al. 2008; Li et al. 2013; Peng et al. 2012).

The enhanced photocatalytic activity under visible light of Cr(III)-doped TiO₂ photocatalysts (relative to the undoped oxide) are most likely due to its higher surface area, mesoporous structure, lower crystallite size, and the presence of defects created in the semiconductor by metal doping. Most of these characteristics are directly related to the preparation method. Because of the higher performance shown by the 0.04-CrTi photocatalyst, this catalyst was selected for further studies aimed to establish the best degradation conditions and intermediates formed.

Effect of catalyst dosage

The effect of catalyst dosage for MCPA degradation was evaluated with three different catalyst quantities of 0.04-CrTi sample: 0.5, 1, and 1.5 g/L under visible radiation. As seen in Fig. 5, the degradation percentage of MCPA increased as the

Table 1. Physicochemical properties of the prepared catalysts

Catalyst	Cr content (wt.%) ^a	Surface area (m ² /g) ^b	Crystallite size (nm) ^c	E _g (eV) ^d
Ti	–	51.5	19.72	3.13
0.02-CrTi	0.012 ± 0.003	56.8	15.25	3.14
0.04-CrTi	0.025 ± 0.002	54.5	14.24	3.14
0.06-CrTi	0.044 ± 0.004	60.4	14.23	3.13

^a Determined by AAS (*n* = 4)

^b BET method

^c Scherrer’s equation applied to the (101) anatase diffraction peak

^d DRS

catalyst dosage was increased to an optimum value of 1 g/L and decreased with increasing catalyst dosage. On one hand, this could be attributed to the effect of catalyst particles that attenuate light absorption inside the reaction medium when the catalyst loading increases above an optimum value. On the other hand, when using a lower catalyst dosage, the number of catalytic active sites in the reaction medium decreased. In both cases, •OH radical production decreased in the photocatalytic system, and therefore, the efficiency of degradation was reduced (Ahmed et al. 2011; Akpan and Hameed 2009).

Effect of radiation source

Sunlight consists of both visible and UV light. From the viewpoint of practical application, it is desirable to develop photocatalysts with high activity under both UV and visible

light in order to utilize sunlight most effectively. Photocatalytic degradation of MCPA using P25, Ti, and 0.04-CrTi was evaluated under both light irradiation sources. Degussa P25 has an E_g value of 3.33 eV, BET surface area of 50 m²/g, and crystallite size of 30 nm (Han et al. 2012; Palominos et al. 2009). The results are shown in Fig. 6a, b. Dark control experiments conducted to determine the exact initial dark adsorption–equilibration period when using 0.04-CrTi as catalyst indicated that MCPA already reached its equilibrium in 1 h with an MCPA removal of approximately 9%. However, MCPA is a photostable herbicide, and photodegradation was negligible in the absence of catalyst under visible and UV light irradiation, obtaining only 4 and 11% degradations of MCPA, respectively. The control experiments (photolysis and adsorption) confirmed that the enhancement in the degradation rate of MCPA is a photocatalytic effect arising from catalyst materials.

The Langmuir–Hinshelwood (L–H) kinetic model has been widely utilized to describe the kinetics of the photocatalytic process (Alvarez-Corena et al. 2016; Dong et al. 2016 Kondarides 2010; Liu et al. 2014). The rate of degradation (*r*) with maximum coverage of sites on the photocatalyst surface

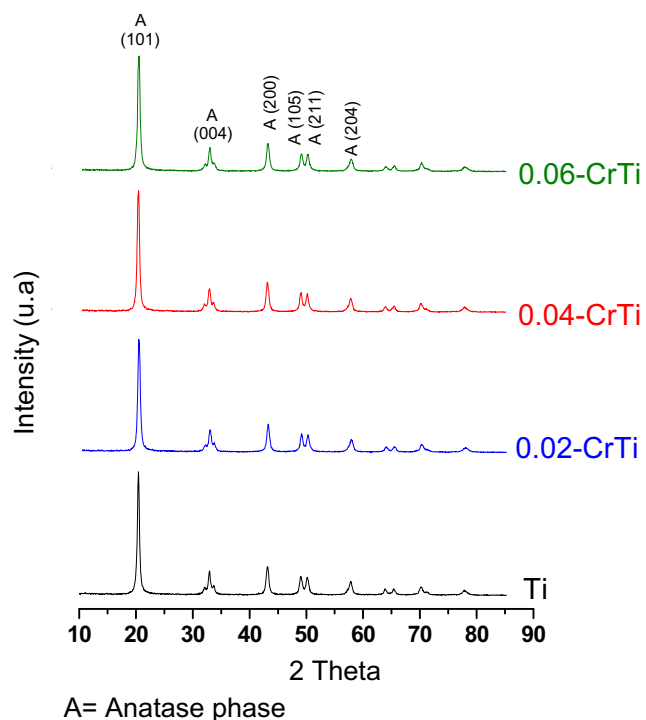


Fig. 1. XRD patterns of the prepared Cr(III)-doped TiO₂ catalysts with various metal doping concentrations

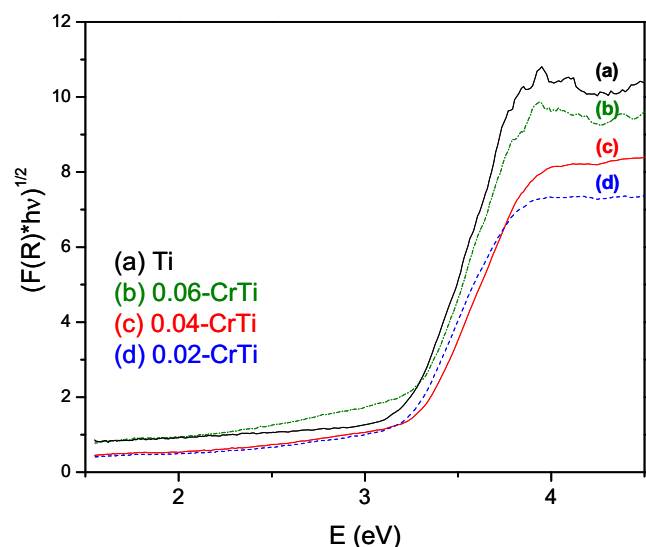


Fig. 2. UV–Vis DRS spectra of the prepared Cr(III)-doped TiO₂ photocatalysts

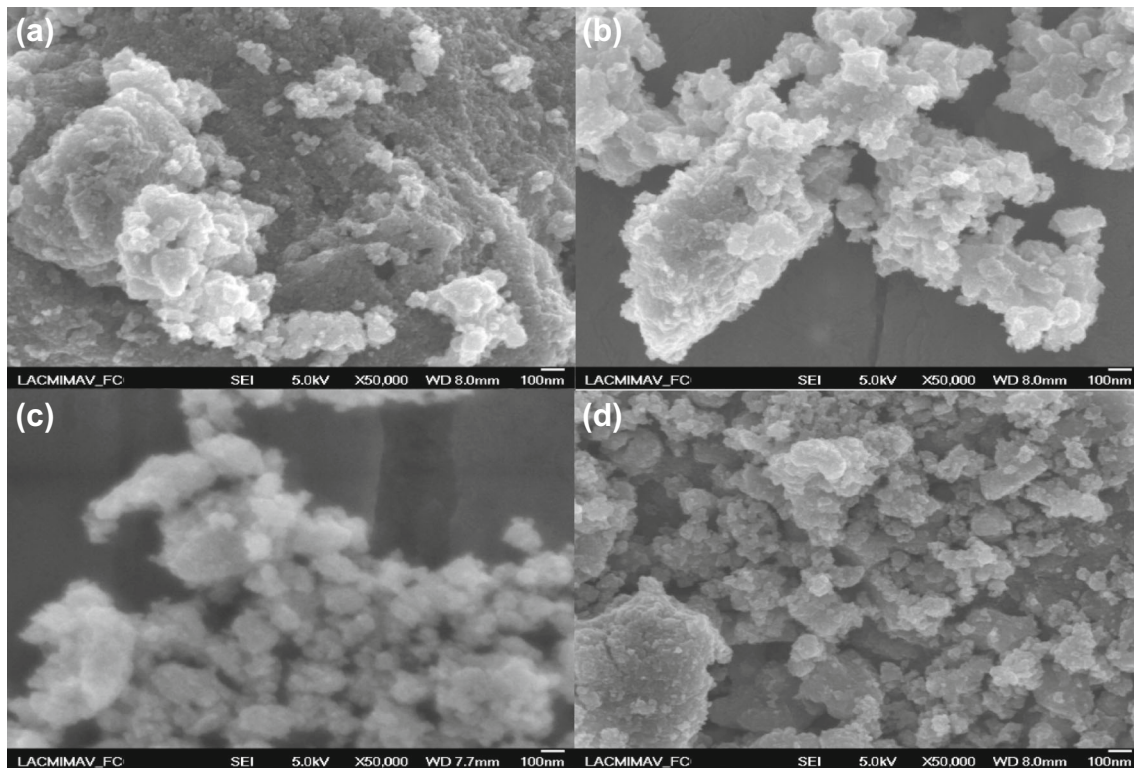


Fig. 3. SEM micrographs at 50,000 \times magnification of the samples: Ti (a), 0.02-CrTi (b), 0.04-CrTi (c), and 0.06-CrTi (d)

is controlled by the reaction rate of the adsorbed molecules and is given by Eq. (3):

$$r = \frac{dc}{dt} = k_{LH} \frac{K_L c}{1 + K_L c}, \quad (3)$$

where K_L is the Langmuir adsorption constant, k_{LH} is the L–H reaction rate constant, and c is the contaminant

concentration. The Langmuir–Hinshelwood (L–H) equation could be simplified considering the possible boundary conditions:

- (a) when $K_L \times c \gg 1$ (at high substrate concentration), the reaction is of pseudo zero order, where k_r is the apparent rate constant:

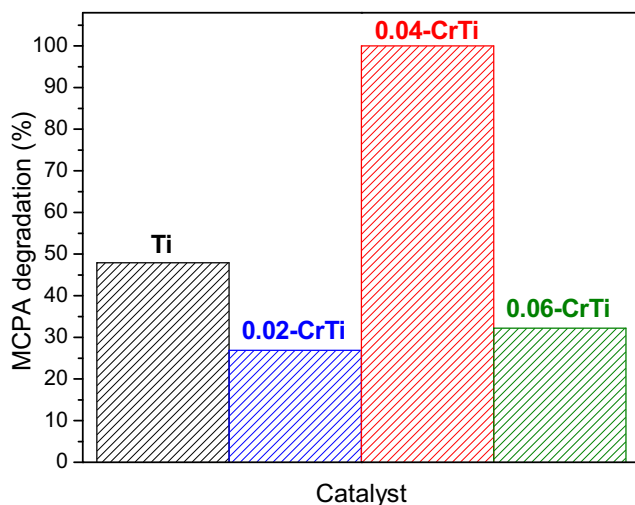


Fig. 4. Comparison of photocatalytic activity under visible radiation for MCPA degradation (10 mg/L) of the undoped and the Cr(III)-doped TiO₂ materials. Experimental conditions: pH 3.5 and 1 g/L of catalyst

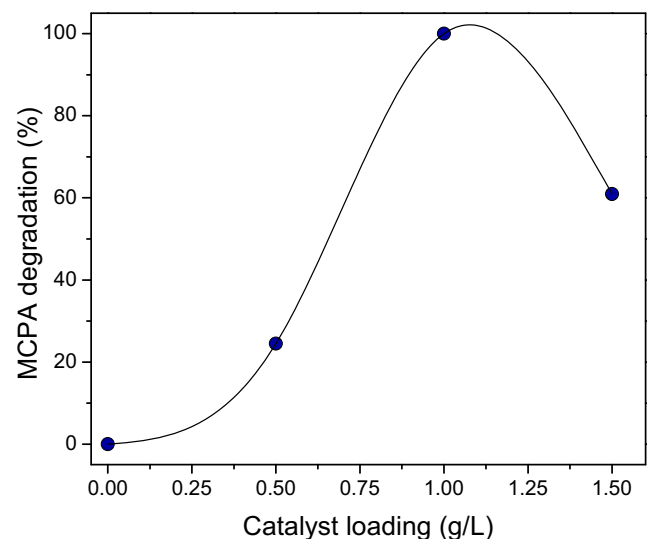


Fig. 5. Effect of the catalyst loading on the degradation of MCPA under visible radiation using 0.04-CrTi (10 mg/L MCPA, pH 3.5)

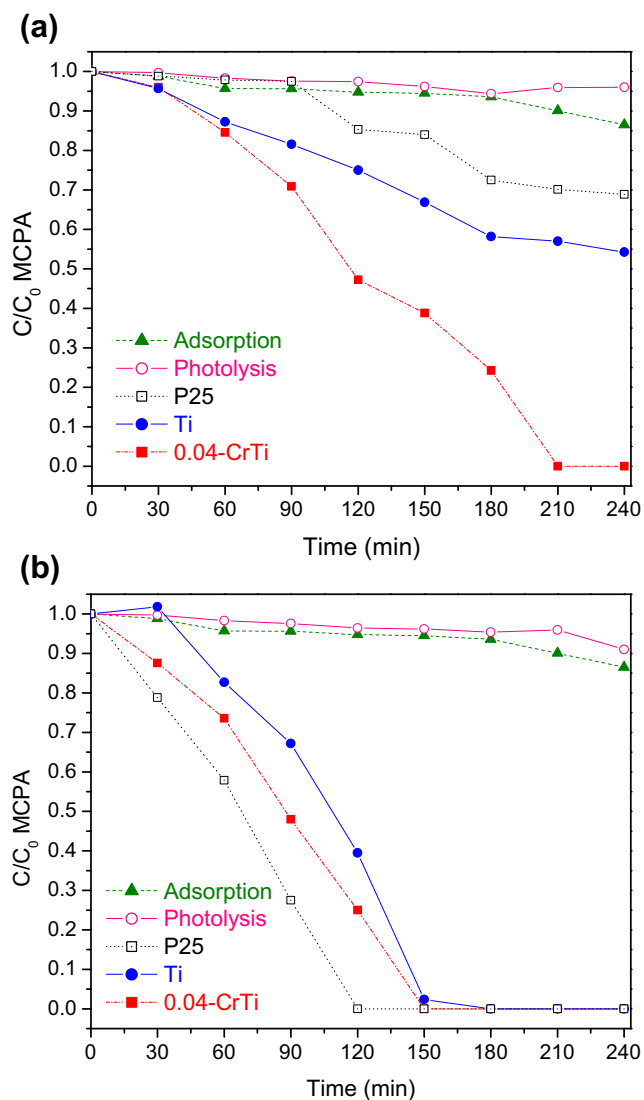


Fig. 6. Adsorption, photolysis, and photocatalytic degradation of MCPA under visible (a) and UV (b) radiation (10 mg/L MCPA, pH 3.5, and 1 g/L of catalyst)

$$r = \frac{dc}{dt} = k_r \tag{4}$$

Integration of Eq. (4) gives the following expression:

$$c - c_0 = -k_r t \tag{5}$$

(b) when $K_L \times c \ll 1$ (for diluted solutions), the reaction is of pseudo-first order. The pseudo-first-order kinetic relationship is shown in Eq. (6), where k_{app} is the apparent rate constant

$$r = \frac{dc}{dt} = k_{app} c \tag{6}$$

Integration gives the following expression:

$$\ln\left(\frac{c}{c_0}\right) = -k_{app} t \tag{7}$$

where c is the MCPA concentration at reaction time t , c_0 is the initial MCPA concentration, and k_{app} is the apparent rate constant. The plot of $\ln(c/c_0)$ versus t gave a straight line, confirming that degradation of MCPA followed pseudo-first-order kinetic.

This model has been commonly accepted to describe photocatalytic processes of organic compounds, including pesticides (Fenoll et al. 2014; Maya-Treviño et al. 2014; Oseghe et al. 2015, Zertal et al. 2004). The apparent rate constants for the evaluated catalysts under visible and UV radiation are included in Table 2. It is worthwhile to mention that the present study was performed at low substrate concentration; therefore, the good correlation of the experimental data (regression coefficients (R^2) between 0.9887 and 0.9977) indicates that photocatalytic degradation of MCPA using these photocatalysts fits into the pseudo-first-order kinetic model.

The photocatalytic degradation of MCPA under visible light radiation (Fig. 6a) indicated that the 0.04-CrTi sample exhibited higher photocatalytic activity compared to that of the Ti and P25 materials, confirming that Cr doping is an effective way to improve the photoactivity of TiO_2 . The MCPA degradation percentages in 240 min were approximately 99, 45, and 32% with 0.04-CrTi, Ti, and P25, respectively. The results revealed that 0.04-CrTi displayed a higher initial rate ($4.1 \times 10^{-3} \text{ min}^{-1}$) of MCPA degradation. The degradation rate under visible radiation with a 0.04% Cr(III) doping concentration was 1.70 and 6.8 times higher compared to that of the bare TiO_2 and P25, respectively. The constant value achieved for MCPA degradation was 3.1 times lower than the k_{app} value ($\sim 15.8 \times 10^{-3} \text{ min}^{-1}$) reported in a previous study using a 0.25 mol% Cr(III)-doped photocatalyst prepared through an aqueous sol-gel method for the photocatalytic oxidation of methylene blue under visible light (Jaimy et al. 2011). Although slightly lower constant rate values were achieved during MCPA degradation using 0.04-CrTi prepared by a microwave-assisted sol-gel method than the reported value on the degradation of azo dye using 0.25 mol% Cr(III)-doped TiO_2 obtained by a sol-gel procedure (Jaimy et al. 2011), there are other operational parameters that could significantly influence the photocatalytic degradation process (e.g., light intensity, nature and concentration of the organic pollutant, nature and loading of photocatalyst) (Dong et al. 2015).

Conversely, under UV irradiation (see Fig. 6b), all the catalysts were effective in removing MCPA; the ordering according to the MCPA degradation rate was as follows: P25 > 0.04-CrTi > Ti.

Table 2. Apparent rate constants and the corresponding linear regression coefficients (R^2) for the photocatalytic degradation of MCPA under UV and visible radiation sources

Catalyst/radiation source	$k_{app} \times 10^3$ (min^{-1})	R^2
P25/Vis	0.6	0.9976
Ti/Vis	2.4	0.9981
0.04-CrTi/Vis	4.1	0.9892
P25/UV	12.3	0.9966
Ti/UV	8.4	0.9977
0.04-CrTi/UV	10.6	0.9887

As observed in Table 2, the MCPA degradation rates were slower under a visible light excitation source when compared to those under the UV light irradiation. Deactivation in the UV region of chromium-doped titania materials prepared under hydrothermal conditions was also described by Ould-Chikh et al. during photocatalytic degradation of formic acid (Ould-Chikh et al. 2014). Thus, the 0.04-CrTi photocatalyst may be good for the degradation of organic molecules under visible light but it requires a longer time for mineralization (total oxidation of MCPA compound to CO_2).

The enhanced photocatalytic activity of Cr(III)-doped TiO_2 under UV and visible radiation depends on the morphological and structural characteristics of the sample as well as on the amount of Cr doping. Doping with 0.04 wt% chromium was mainly responsible for the efficient separation of photogenerated electrons and holes in the TiO_2 under UV radiation, preventing the electron-hole pair recombination. While using visible radiation, Cr(III) ions increased absorption in the visible light region of the spectra, resulting in production of more photogenerated electron/hole pairs that could participate in redox reactions improving the photoreactivity of Cr(III)-doped TiO_2 (Peng et al. 2012; Zhu et al. 2006).

Intermediate products generated under UV and visible radiation

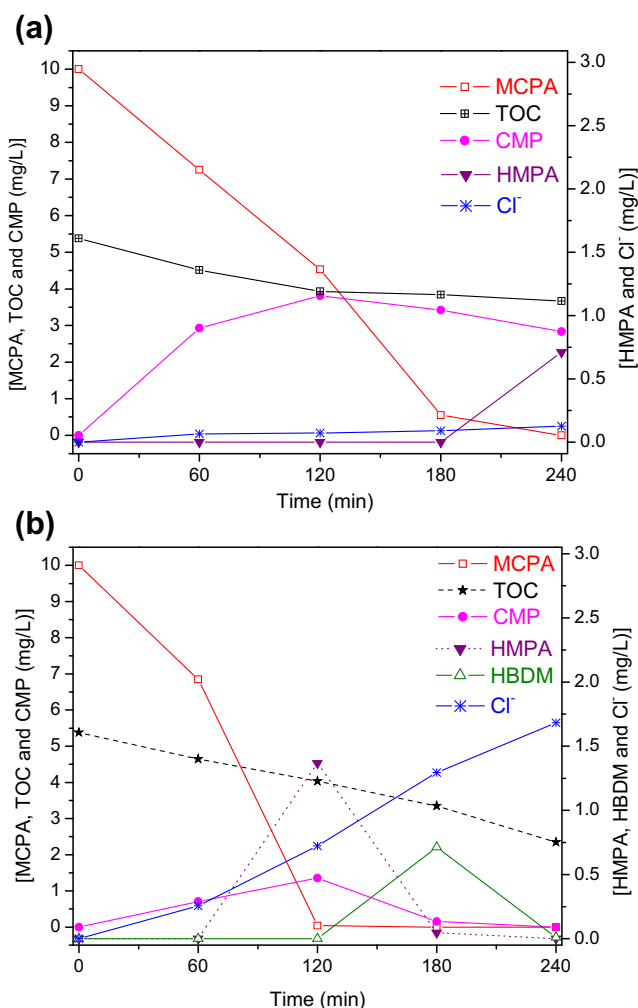
The intermediates formed, the end-product Cl^- generated, and the mineralization abatement during the photocatalytic degradation of MCPA in aqueous suspensions of 0.04-CrTi under visible (Fig. 7a) and UV radiation (Fig. 7b) were determined by GC-MS, ion chromatography, and TOC analysis, respectively.

The intermediates detected were 4-chloro-2-methylphenol (CMP), 2-(4-hydroxy-2-methylphenoxy) acetic acid (HMPA), and 2-hydroxybuta-1,3-diene-1,4-diyl-bis(oxy)dimethanol (HBDM).

Only aromatic intermediates CMP and HMPA were identified during the visible light-mediated photocatalytic degradation of MCPA, which were not completely removed after

240 min (see Fig. 7a). CMP was generated from MCPA by the attack of $\cdot\text{OH}$ on the C(1)-O bond and reached a maximum concentration of 4 mg/L in 120 min. The hydroxylation of MCPA by a photo-induced hydroxyl radical with dechlorination formed HMPA and a Cl^- ion. CMP is more toxic than the parent compound and is listed in the priority pollutant list of the European Community as more hazardous to human health (Solís et al. 2015). Thus, the quantification of this intermediate should be taken into consideration during water treatment related with the MCPA removal. Visible light 0.04-CrTi mediated photocatalytic treatment resulted in 32% mineralization.

Conversely, photocatalytic degradation under UV radiation with 0.04-CrTi material generated the aromatic intermediates CMP and HMPA that were completely removed in 180 min, after reaching maxima of 1.35 and 1.38 mg/L, respectively (see Fig. 7b). The UV-mediated photocatalytic reaction led

**Fig. 7.** Photocatalytic degradation and mineralization of MCPA: evolution of the Cl^- ion as an end-product and CMP, HMPA, and HBDM intermediates formed using the 0.04-CrTi catalyst under visible (a) and UV (b) radiation

to the complete removal of the aromatic intermediates; however, the herbicide was not completely mineralized and some intermediates accumulated in the reaction media. The 2-hydroxybuta-1,3-diene-1,4-diyl-bis(oxy)dimethanol (HBDM) was identified during UV photocatalytic degradation of MCPA. HBDM was formed by demethylation and ring opening of HMPA. As shown in Fig. 7b, after 180 min, ~56% of TOC percentage was achieved. The degradation of MCPA was accompanied by the loss of its initial chlorine (1.77 mg/L) as Cl^- ion, as confirmed by ionic chromatography. As seen in Fig. 7b, the Cl^- ion generated in 240 min of reaction was approximately 1.68 mg/L (94.9% of initial Cl^- concentration). The formation of the main intermediate CMP has been described during degradation of MCPA by TiO_2 -mediated photocatalysis treatment (Djebbar et al. 2006; Oseghe et al. 2015; Zertal et al. 2004), UVA/ TiO_2/O_3 system (Solis et al. 2015), and photoelectron-Fenton processes (Garcia-Segura et al. 2011). Conversely, intermediate compounds such as HMPA and HBDM, with significantly lower toxicity than MCPA and CMP, have been mainly described during the TiO_2 -mediated photocatalysis process (Djebbar et al. 2006; Oseghe et al. 2015).

Conclusions

Cr(III)-doped TiO_2 materials with Cr(III) doping contents of 0.02, 0.04, and 0.06 wt% have been prepared by a MW-assisted sol-gel procedure. In all cases, the obtained materials had an anatase structure and small crystalline size, high surface area, mesoporous structure, enhanced absorption in the visible region, and surface defects created by metal doping from the preparation method that prevents charge recombination of the electrons and holes. They also exhibited a visible light-induced activity due to the transition from the TiO_2 valence band to the Cr(III) impurity states. The Cr(III)-doped TiO_2 catalyst with 0.04 wt% Cr(III) showed higher photocatalytic performance than the bare TiO_2 for the degradation of MCPA under both UV and visible light radiation, which is attributed to the synergistic effect of the morphology, composition, structure, and optical properties. Intermediates of MCPA degradation were identified as 4-chloro-2-methylphenol, 2-(4-hydroxy-2-methylphenoxy) acetic acid, and 2-hydroxybuta-1,3-diene-1,4-diyl-bis(oxy)dimethanol. TOC analysis confirmed the mineralization of MCPA with 32 and 56% removal by visible light- and UV-mediated 0.04-CrTi photocatalysts, respectively. The toxicity of intermediate products generated during the MCPA degradation depended on the irradiation source and, in contrast to the initial MCPA, might be mineralized using biological treatment methods.

Acknowledgments The authors gratefully acknowledge the financial support from the National Council of Science and Technology, Mexico (CONACyT, project 181057), PAICYT UANL 2015, and Facultad de Ciencias Químicas, UANL. Mendiola-Alvarez thanks CONACyT for the scholarship granted. The Spanish Ministerio de Economía y Competitividad (MINECO) and the European Funds for Regional Development (FEDER) are also gratefully acknowledged for the financial support through Project CTQ2013-47461-R.

References

- Ahmed S, Rasul MG, Brown R, Hashib MA (2011) Influence of parameters on the heterogeneous photocatalytic degradation of pesticides and phenolic contaminants in wastewater: a short review. *J Environ Manag* 92:311–330
- Akpan UG, Hameed BH (2009) Parameters affecting the photocatalytic degradation of dyes using TiO_2 -based photocatalysts: a review. *J Hazard Mater* 170:520–529
- Alvarez-Corena JR, Bergendahl JA, Hart FL (2016) Advanced oxidation of five contaminants in water by UV/ TiO_2 : reaction kinetics and byproducts identification. *J Environ Manag* 181:544–551
- Daghrir R, Drogui P, Robert D (2013) Modified TiO_2 for environmental photocatalytic applications: a review. *Ind Eng Chem Res* 52:3581–3599
- Devi LG, Kumar SG (2011) Influence of physicochemical–electronic properties of transition metal ion doped polycrystalline titania on the photocatalytic degradation of indigo carmine and 4-nitrophenol under UV/solar light. *Appl Surf Sci* 257:2779–2790
- Devi LG, Kavitha R (2013) A review on non metal ion doped titania for the photocatalytic degradation of organic pollutants under UV/solar light: role of photogenerated charge carrier dynamics in enhancing the activity. *Appl Catal B Environ* 140–141:559–587
- Djebbar K, Zertal A, Sehili T (2006) Photocatalytic degradation of 2,4-dichlorophenoxyacetic acid and 4-chloro-2-methylphenoxyacetic acid in water by using TiO_2 . *Environ Technol* 27:1191–1197
- Dong H, Zeng G, Tang L, Fan C, Zhang C, He X, He Y (2015) An overview on limitations of TiO_2 -based particles for photocatalytic degradation of organic pollutants and the corresponding countermeasures. *Water Res* 79:128–146
- Dong R, Na C, Wang X, Zhang H, Li Z, Chen Z, Jin C (2016) Sequential growth of rutile TiO_2 nanorods and anatase TiO_2 nanoparticles on $\text{TiO}_2/\text{SiO}_2$ template spheres. *Mater Chem Phys* 174:81–90
- Fan X, Chen X, Zhu S, Li Z, Yu T, Ye J, Zou Z (2008) The structural, physical and photocatalytic properties of the mesoporous Cr-doped TiO_2 . *J Mol Catal A Chem* 284:155–160
- Fenoll J, Vela N, Garrido I, Perez-Lucas G, Navarro S (2014) Abatement of spinosad and indoxacarb residues in pure water by photocatalytic treatment using binary and ternary oxides of Zn and Ti. *Environ Sci Pollut Res Int* 21:12143–12153
- Garcia-Segura S, Almeida LC, Bocchi N, Brillas E (2011) Solar photoelectro-Fenton degradation of the herbicide 4-chloro-2-methylphenoxyacetic acid optimized by response surface methodology. *J Hazard Mater* 194:109–118
- Gimeno O, Aguinaco A, Rey A, Beltrán Novillo FJ, Toledo JR (2014) Ozonation of 4-chloro-2-methylphenoxyacetic acid (MCPA) in an activated sludge system. *J Chem Technol Biotechnol* 89:1219–1227
- Gupta S, Tripathi M (2012) A review on the synthesis of TiO_2 nanoparticles by solution route. *Open Chem* 10:279–294
- Han J, Liu Y, Singhal N, Wang L, Gao W (2012) Comparative photocatalytic degradation of estrone in water by ZnO and TiO_2 under artificial UVA and solar irradiation. *Chem Eng J* 213:150–162

- Jaimy KB, Ghosh S, Sankar S, Warriar KGK (2011) An aqueous sol–gel synthesis of chromium(III) doped mesoporous titanium dioxide for visible light photocatalysis. *Mater Res Bull* 46:914–921
- Kamaraj R, Davidson DJ, Sozhan G, Vasudevan S (2014) An in situ electrosynthesis of metal hydroxides and their application for adsorption of 4-chloro-2-methylphenoxyacetic acid (MCPA) from aqueous solution. *J Environ Chem Eng* 2:2068–2077
- Kaminski W, Kusmirek K, Swiatkowski A (2014) Sorption equilibrium prediction of competitive adsorption of herbicides 2,4-D and MCPA from aqueous solution on activated carbon using ANN. *Adsorption* 20:899–904
- Kondarides DI (2010): Catalysis In: Centi G (Editor), Photocatalysis Encyclopedia of life support systems (EOLSS) (<http://www.eolss.net>). Eolss, Oxford, UK, pp. 1–97
- Li X, Guo Z, He T (2013) The doping mechanism of Cr into TiO₂ and its influence on the photocatalytic performance. *Phys Chem Chem Phys* 15:20037–22045
- Liu B, Zhao X, Terashima C, Fujishima A, Nakata K (2014) Thermodynamic and kinetic analysis of heterogeneous photocatalysis for semiconductor systems. *Phys Chem Chem Phys*: PCCP 16:8751–8760
- López R, Gómez R (2011) Band-gap energy estimation from diffuse reflectance measurements on sol–gel and commercial TiO₂: a comparative study. *J Sol-Gel Sci Technol* 61:1–7
- Maya-Treviño ML, Guzmán-Mar JL, Hinojosa-Reyes L, Ramos-Delgado NA, Maldonado MI, Hernández-Ramírez A (2014) Activity of the ZnO–Fe₂O₃ catalyst on the degradation of Dicamba and 2,4-D herbicides using simulated solar light. *Ceram Int* 40:8701–8708
- Michalow KA, Otal EH, Burnat D, Fortunato G, Emerich H, Ferri D, Heel A, Graule T (2013) Flame-made visible light active TiO₂:Cr photocatalysts: correlation between structural, optical and photocatalytic properties. *Catal Today* 209:47–53
- Muter O, Berzins A, Strikauska S, Pugajeva I, Bartkevics V, Dobele G, Truu J, Truu M, Steiner C (2014) The effects of woodchip- and straw-derived biochars on the persistence of the herbicide 4-chloro-2-methylphenoxyacetic acid (MCPA) in soils. *Ecotoxicol Environ Saf* 109:93–100
- Oseghe EO, Ndungu PG, Jonnalagadda SB (2015) Photocatalytic degradation of 4-chloro-2-methylphenoxyacetic acid using W-doped TiO₂. *J Photochem Photobiol A Chem* 312:96–106
- Ould-Chikh S, Proux O, Afanasiev P, Khrouz L, Hedhili MN, Anjum DH, Harb M, Geantet C, Basset JM, Puzenat E (2014) Photocatalysis with chromium-doped TiO₂: bulk and surface doping. *ChemSusChem* 7:1361–1371
- Palominos RA, Mondaca MA, Giraldo A, Peñuela G, Pérez-Moya M, Mansilla HD (2009) Photocatalytic oxidation of the antibiotic tetracycline on TiO₂ and ZnO suspensions. *Catal Today* 144:100–105
- Pan LK, Liu XJ, Sun Z, Sun CQ (2013) Nanophotocatalysts via microwave-assisted solution-phase synthesis for efficient photocatalysis. *J Mater Chem A* 1:8299–8326
- Pelaez M, Nolan NT, Pillai SC, Seery MK, Falaras P, Kontos AG, Dunlop PSM, Hamilton JJJ, Byrne JA, O’Shea K, Entezari MH, Dionysiou DD (2012) A review on the visible light active titanium dioxide photocatalysts for environmental applications. *Appl Catal B Environ* 125:331–349
- Peng Y-H, Huang G-F, Huang W-Q (2012) Visible-light absorption and photocatalytic activity of Cr-doped TiO₂ nanocrystal films. *Adv Powder Technol* 23:8–12
- Rodríguez Pereiro I, González Irimia R, Rubí Cano E, Cela Torrijos R (2004) Optimisation of a gas chromatographic–mass spectrometric method for the determination of phenoxy acid herbicides in water samples as silyl derivatives. *Anal Chim Acta* 524:249–256
- Sanchis S, Polo AM, Tobajas M, Rodríguez JJ, Mohedano AF (2013) Degradation of chlorophenoxy herbicides by coupled Fenton and biological oxidation. *Chemosphere* 93:115–122
- Solís RR, Rivas FJ, Pérez-Bote JL, Gimeno O (2015) Photocatalytic ozonation of 4-chloro-2-methylphenoxyacetic acid and its reaction intermediate 4-chloro-2-methyl phenol. *J Taiwan Inst Chem Eng* 46: 125–131
- Tian B, Li C, Zhang J (2012) One-step preparation, characterization and visible-light photocatalytic activity of Cr-doped TiO₂ with anatase and rutile bicrystalline phases. *Chem Eng J* 191:402–409
- United States Environmental Protection Agency U (2004) Reregistration Eligibility Decision (RED) for MCPA (2-methyl-4-chlorophenoxyacetic acid) List A Case 0017. In: USEPA USEPA (Hrsg.). Office of Pesticide Programs (OPP), Washington, D.C. 20460, pp. 1–72
- Vijayalakshmi K, Jereil SD (2015) Effect of Cr incorporation on the properties of TiO₂ nanoparticles synthesized by microwave technique. *J Mater Sci Mater Electron* 26:3790–3796
- WHO WHO (2006) Guías para la calidad del agua potable: recomendaciones., Geneva, Switzerland, pp. 398 p
- Wu C-H, Kuo C-Y, Lin C-J, Chiu P-K (2013) Preparation of N-TiO₂ using a microwave/sol-gel method and its photocatalytic activity for bisphenol A under visible-light and sunlight irradiation. *Int J Photoenergy* 2013:1–9
- Wu Y-C, Tai Y-C (2013): Effects of alcohol solvents on anatase TiO₂ nanocrystals prepared by microwave-assisted solvothermal method. *J Nanopart Res* 15
- Zertal A, Molnár-Gábor D, Malouki MA, Sehili T, Boule P (2004) Photocatalytic transformation of 4-chloro-2-methylphenoxyacetic acid (MCPA) on several kinds of TiO₂. *Appl Catal B Environ* 49: 83–89
- Zhu J, Deng Z, Chen F, Zhang J, Chen H, Anpo M, Huang J, Zhang L (2006) Hydrothermal doping method for preparation of Cr³⁺-TiO₂ photocatalysts with concentration gradient distribution of Cr³⁺. *Appl Catal B Environ* 62:329–335